Hindawi
Journal of Advanced Transportation
Volume 2022, Article ID 7344044, 15 pages
https://doi.org/10.1155/2022/7344044

Research Article

Research on Lateral and Longitudinal Coordinated Control of Distributed Driven Driverless Formula Racing Car under High-Speed Tracking Conditions

Yunlong Bai,[1] **Gang Li**,[1] **Hongyao Jin**,[1] **and Ning Li**[2]

[1]*School of Automobile and Traffic Engineering, Liaoning University of Technology, Jinzhou 121001, China*
[2]*School of Electronics & Information Engineering, Liaoning University of Technology, Jinzhou 121001, China*

Correspondence should be addressed to Gang Li; qcxyligang@lnut.edu.cn

Received 20 April 2022; Revised 10 July 2022; Accepted 12 July 2022; Published 11 August 2022

Academic Editor: Saber Fallah

Aiming at the problem that it is difficult to ensure the trajectory tracking accuracy and driving stability of the distributed driven driverless formula racing car under high-speed tracking conditions, a lateral and longitudinal coordinated control strategy is proposed. Based on the adaptive model predictive control theory, the lateral motion controller is designed, and the prediction time domain of the controller is changed in real time according to the change of vehicle speed. Based on the sliding mode variable structure control theory, a longitudinal motion controller is designed to accurately track the desired vehicle speed. Considering the coupling between the lateral and longitudinal controls, the lateral controller inputs the longitudinal speed and displacement of the vehicle, using the feedback mechanism to update the prediction model in real time, the longitudinal controller takes the front wheel angle as the input, the driving torque is redistributed through the differential drive control, and the lateral and longitudinal coordinated control is carried out to improve the trajectory tracking accuracy and driving stability. The typical working conditions are selected for co-simulation test verification. The results show that the lateral and longitudinal coordinated control strategy can effectively improve the vehicle trajectory tracking control accuracy and driving stability.

1. Introduction

High-speed tracking is a competition item in the driverless formula competition. The track layout of this project is a closed-loop path composed of multiple sections of variable curvature curves and part of straights, and the route is relatively complex. When the racing car is driving on a straight road, it needs to pass the straight part at the fastest speed, and when entering a corner, it needs to slow down appropriately and pass the corner at a safe speed. Under the condition of high-speed tracking, the racing car must drive on the track with complex and changeable curvature at a high speed, and cannot hit the pile barrels on both sides of the track, which puts forward higher requirements for the trajectory tracking control of the racing car. There is a strong coupling relationship between the lateral and longitudinal directions when the racing car is running at high speed. The lateral or longitudinal control alone cannot meet the trajectory tracking requirements of the racing car. Therefore, it is necessary to design a lateral and longitudinal coordinated control strategy to improve the accuracy of trajectory tracking and driving stability.

A large number of scholars at home and abroad have conducted in-depth research on the trajectory tracking control of driverless vehicles. The commonly used trajectory tracking control theories include pure tracking control [1, 2], fuzzy control [3], optimal control [4], model prediction control [5, 6], sliding mode variable structure control [7], and so on. Most of the early trajectory tracking control is to separate the lateral motion from the longitudinal motion, and use different methods to improve the accuracy of the lateral and longitudinal motion control. In order to improve the accuracy of lateral motion control, Carlucho et al. [8] designed an adaptive MIMO-PID controller based on

reinforcement learning for uncertainties in complex scenarios, which improved the accuracy of lateral control. Zhang et al. [9] proposed a fuzzy observer-based output feedback controller design method, but this method relies too much on the rule base, which will lead to the inability to fully utilize the motion performance of the vehicle. Kapania and Gerdes [10] designed a feedback-feedforward lateral motion controller to reduce the lateral position tracking error and improve the steering stability, but this method is not suitable for vehicles with variable speeds. Pinto et al. [11] proposed an optimal trajectory tracking control strategy based on multiple constraints, which obtained good trajectory tracking accuracy by continuously linearizing the error model and using quadratic programming to solve. Novil et al. [12] proposed a hierarchical control method of nonlinear model predictive control (NMPC), the high-order MPC calculates the curve of optimal speed and the low-order NMPC constrains the motion curve, and the real-time performance of the control algorithm is improved. Zhang et al. [13] proposed an adaptive MPC controller based on the recursive least squares method, which can achieve better tracking results under different driving conditions. In order to improve the tracking accuracy and stability of longitudinal motion control, Kim [14] et al. designed an adaptive drive-by-wire and brake-by-wire control algorithm that can overcome the changing vehicle parameters. Velenis and Tsiotras [15] used an optimal control method to constrain the acceleration to increase the lap time of the car in order to obtain the optimal driving speed. Buechel and Knoll [16] proposed a longitudinal control algorithm based on adaptive vehicle state and parameter observer, and used KF (Kalman filtering) to design a real-time vehicle state observer that can quickly adapt to changes in vehicle parameters.

However, in some complex working conditions, a single lateral control or longitudinal control cannot obtain high trajectory tracking accuracy, and the interaction between lateral and longitudinal controls needs to be considered. Therefore, some scholars improve the accuracy of trajectory tracking through lateral and longitudinal coordinated control. Xu et al. [17] designed a lateral and longitudinal controller based on the preview-follower theory (PFT) and MPC theory. PFT updated the reference value according to the preview point and controlled the transverse and longitudinal motion of the vehicle through MPC, achieving a good tracking effect. Xie and Liu [18] proposed a transverse and longitudinal collaborative control method based on model predictive control theory. The longitudinal control calculates the expected acceleration through MPC, and then uses the inverse longitudinal dynamic model to coordinate driving and braking. The transverse motion solves the front wheel angle according to the vehicle state and longitudinal speed, so as to realize the stable tracking of the vehicle. Zhang and Li [19] designed a method of linear quadratic regulator (LQR) and dual PID lateral and longitudinal coordinated control considering feedforward control and angle compensation. The LQR controller is used as the lateral controller, and the longitudinal control adopts dual PID controllers to control the vehicle speed, which has a better tracking effect. Qin et al. [20] designed a lateral and longitudinal coordinated controller for the lateral and longitudinal coordinated control of vehicle following and path tracking during the driving process of the intelligent networked fleet, considering the coupling characteristics of the vehicle's longitudinal and lateral motion, but only the effect of longitudinal speed on lateral controller is considered. Chen et al. [21] proposed a lateral and longitudinal coordinated control method based on nonlinear model predictive control (NMPC) in the face of large curvature turns of driverless vehicles; the NMPC is combined with the obstacle function, and the expected longitudinal force, lateral force, and yaw moment are calculated through NMPC, and then the optimal distribution of the four-wheel tire force is solved through the obstacle function to control the lateral and longitudinal motion of the driverless vehicle, effectively reducing the track tracking error.

To sum up, scholars have done some studies on the lateral and longitudinal coordinated control of driverless vehicles. At present, most of the researches are focused on the driverless cars under normal driving conditions, but there are few researches on the distributed drive driverless racing car under high-speed tracking conditions. Therefore, this paper studies the lateral and longitudinal coordinated control of distributed drive driverless racing car under high-speed tracking condition, and proposes a lateral and longitudinal coordinated control strategy. Through the coordinated control of lateral and longitudinal motion, the driving stability and safety of driverless racing car under high-speed tracking condition can be improved. The outstanding contributions of the paper are summarized as follows:

(i) Based on the traditional model predictive control (MPC) theory, the influence relationship between longitudinal speed, prediction time domain, and MPC controller output was studied, and an adaptive model predictive control (MPC) algorithm was proposed which could change the prediction time domain in real time according to the change of vehicle speed.

(ii) Based on sliding mode variable structure control theory, the longitudinal motion controller of racing car is designed, and the driving torque is redistributed by differential drive.

(iii) Considering the coupling relationship between Lateral and Longitudinal control, a Lateral and Longitudinal cooperative control strategy is proposed. The lateral controller inputs the longitudinal velocity and displacement of the vehicle as state variables and uses feedback mechanism to update the prediction model in real time. The longitudinal controller inputs the front wheel angle of the racing car, considers the influence of lateral force, and redistributes the control torque in the form of differential drive.

The remainder of this paper is organized as follows. In Section 2, the 3-DOF vehicle dynamics model is introduced. In Section 3, the Lateral and Longitudinal

cooperative control strategy is designed. The Lateral motion controller is designed based on MPC theory, and the longitudinal motion controller is designed based on SMC theory. In section 4, the differential drive control strategy is introduced. The simulation results are discussed in Section 5. The conclusions and future work of this paper are discussed in Section 6.

2. Establishment of the Vehicle Dynamics Model

In order to more accurately describe the vehicle's lateral and longitudinal motion states and dynamic characteristics, and at the same time to reduce the calculation amount in the process of solving the vehicle dynamics model, a three-degree-of-freedom dynamic model that only considers the longitudinal, lateral, and yaw motions of the vehicle is established as the reference model of the controller, as shown in Figure 1. The following simplifications are made: the road surface is assumed to be smooth and the vertical motion of the vehicle is ignored; the vehicle suspension system and aerodynamics are ignored; the lateral load transfer of the tires is ignored.-Where XOY is the geodetic coordinate system; xoy is the vehicle coordinate system; a, b is the distance from the center of mass to the front and rear axles; $\dot{x}$ and $\dot{y}$ is the speed of the vehicle in the x and y axis direction, respectively; $\dot{\varphi}$ is the vehicle yaw rate; δ_f is the front wheel angle; F_{lf} and F_{lr} is the longitudinal force of the front tire and rear tire, respectively; F_{cf} and F_{cr} is the lateral force of the front tire and rear tire, respectively; and α_f and α_r is the front and rear tire slip angle, respectively. According to Newton's second law, the force balance equations of the x and y axles and the moment balance equations around the z axis are obtained, respectively:

$$\begin{cases} m\ddot{x} = 2F_{xf} + 2F_{xr} + m\dot{y}\dot{\varphi}, \\ m\ddot{y} = 2F_{yf} + 2F_{yr} - m\dot{x}\dot{\varphi}, \\ I_z\ddot{\varphi} = 2aF_{yf} - 2bF_{yr}, \end{cases} \tag{1}$$

where m is the vehicle mass; $\ddot{x}$ and $\ddot{y}$ is the acceleration of the vehicle in the x and y axis direction, respectively; I_z is the moment of inertia of the vehicle; and $\ddot{\varphi}$ is the yaw angle acceleration.

During the driving process of the vehicle, only the tires generate force through contact with the ground, which provides the force required for the vehicle to move forward and turn. Therefore, the tire force cannot be ignored. In this paper, the simplified "magic formula" tire model is selected to analyze the tire force, and the small angle assumption is adopted. The lateral force and longitudinal force of the front and rear tires are expressed as:

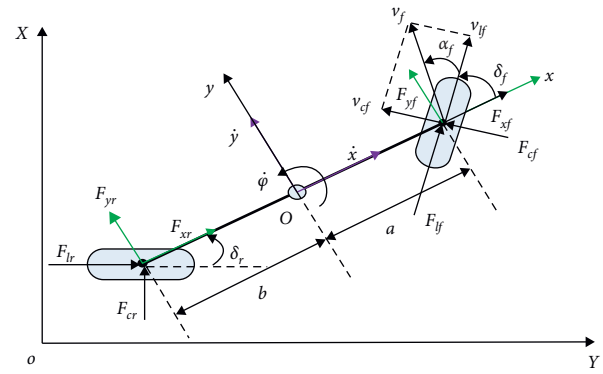

Figure 1: Three-degree-of-freedom nonlinear dynamic model.

$$\begin{cases} F_{lf} = C_{lf}S_f, \\ F_{lr} = C_{lr}S_r, \\ F_{cf} = C_{cf}\alpha_f = C_{cf}\left(\delta_f - \dfrac{\dot{y} + a\dot{\varphi}}{\dot{x}}\right), \\ F_{cr} = C_{cr}\alpha_r = C_{cr}\left(\dfrac{b\dot{\varphi} - \dot{y}}{\dot{x}}\right), \end{cases} \tag{2}$$

where C_{lf} and C_{lr} are the longitudinal stiffness of front and rear tires; C_{cf} and C_{cr} are the lateral stiffness of front and rear tires; S_f and S_r are the slip rate of the front and rear tires.

Finally, according to Newton's second law, the transformation between vehicle coordinate system and geodetic coordinate system, and the tire force analysis, the vehicle dynamics equation is:

$$\begin{cases} \ddot{x} = \dfrac{2}{m}\left[C_{lf}S_f - C_{cf}\left(\delta_f - \dfrac{\dot{y} + a\dot{\varphi}}{\dot{x}}\right)\delta_f + C_{lr}S_r\right] + \dot{y}\dot{\varphi}, \\ \ddot{y} = \dfrac{2}{m}\left[C_{cf}\left(\delta_f - \dfrac{\dot{y} + a\dot{\varphi}}{\dot{x}}\right) + C_{cr}\left(\dfrac{b\dot{\varphi} - \dot{y}}{\dot{x}}\right)\right] - \dot{x}\dot{\varphi}, \\ \ddot{\varphi} = \dfrac{2}{I_z}\left[a\left(C_{cf}\left(\delta_f - \dfrac{\dot{y} + a\dot{\varphi}}{\dot{x}}\right) - bC_{cr}\left(\dfrac{b\dot{\varphi} - \dot{y}}{\dot{x}}\right)\right)\right], \\ \dot{Y} = \dot{x}\sin\varphi + \dot{y}\cos\varphi, \\ \dot{X} = \dot{x}\cos\varphi - \dot{y}\sin\varphi, \end{cases} \tag{3}$$

where $\dot{X}$ and $\dot{Y}$ is the speed of the vehicle in the X and Y axis directions of the inertial coordinate system, respectively.

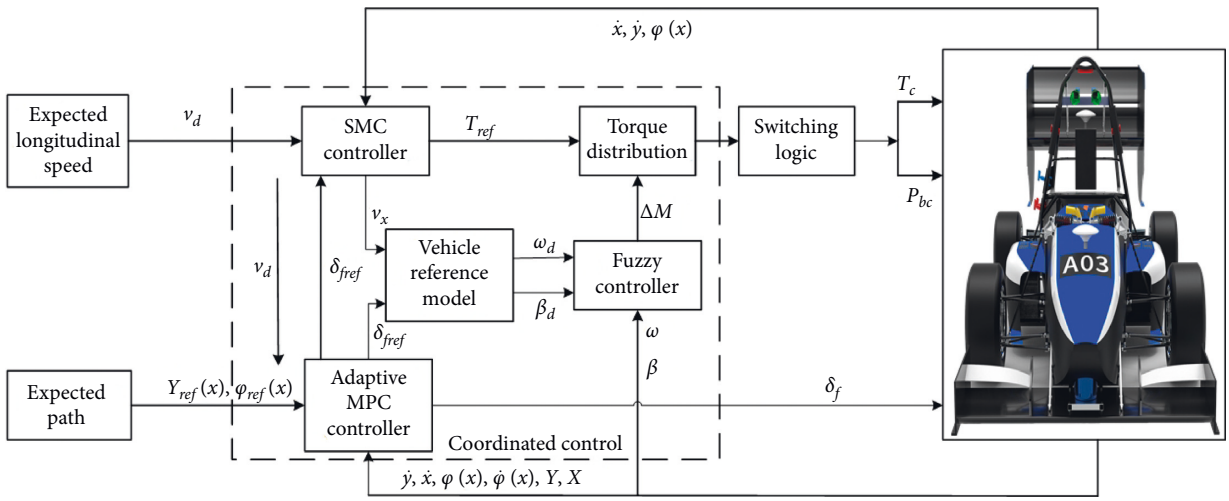

Figure 2: Lateral and longitudinal collaborative control strategy.

3. Lateral and Longitudinal Coordinated Control

In the process of high-speed driving, the vehicle has a strong coupling relationship between the lateral and longitudinal directions. To achieve high-precision trajectory tracking, the interaction between the lateral and longitudinal directions cannot be ignored, and it is necessary to coordinate control of lateral and longitudinal. The lateral and longitudinal coordinated control strategy proposed in this paper is shown in Figure 2. The lateral control is based on the model predictive control theory, and an adaptive model predictive control algorithm is designed to track the desired trajectory; the longitudinal control adopts the sliding mode variable structure control theory to track the desired vehicle speed. In the lateral control, in addition to inputting the desired trajectory and the vehicle lateral state quantity, the longitudinal speed and longitudinal displacement of the vehicle are also used as inputs, the adaptive MPC controller can change the prediction time domain of the model predictive control in real time according to the longitudinal input to improve the lateral tracking effect, the longitudinal controller adds the influence of lateral force, and the front wheel angle output by the lateral controller is used as the input of the longitudinal controller. The resultant torque of the racing car is calculated by the front wheel Angle and the expected speed, and the driving and braking switching logic of the racing car is designed according to the calculated resultant torque to realize the acceleration and deceleration. The additional yaw moment of the racing car is calculated by fuzzy control, and the additional yaw moment is redistributed by differential drive according to the rules. The accuracy of vehicle track tracking and driving stability was improved by lateral and longitudinal coordinated control.

3.1. Lateral Controller Design. The lateral controller is designed based on the model predictive control theory. The model predictive control can predict the output of the system in the future according to the prediction model, the current state quantity of the system and the future control quantity, and can solve problems with various constraints in a rolling manner. The MPC control process mainly includes the establishment of the prediction model, the deduction of the prediction equation, the design of the objective function, the addition of constraints, and the rolling optimization solution [22].

Convert the three-degree-of-freedom model of the vehicle to a state-space representation:

$$\begin{cases} \dot{\xi} = f(\xi, u), \\ \lambda = C \cdot \xi, \end{cases} \tag{4}$$

where ξ is the state quantity, $\xi = [\dot{y}, \dot{x}, \varphi, \dot{\varphi}, Y, X]^T$; u is the control quantity, $u = [\delta_f]$; λ is the output, $\lambda = [\varphi, Y]^T$.

The three-degree-of-freedom model of the vehicle is a nonlinear model, which is linearized. (4) is expanded at point $[\xi_0, u_0]$ using Taylor's formula; retaining the first-order term yields a linear time-varying equation:

$$\dot{\xi} = f(\xi_0, u_0) + A(t)(\xi - \xi_0) + B(t)(u - u_0), \tag{5}$$

where $A(t)$ is the $f(\xi, u)$ Jacobian matrix for ξ; $B(t)$ is the $f(\xi, u)$ Jacobian matrix for u.

The first-order quotient difference is used to discretize (5) to obtain the discrete state space equation:

$$\xi(k+1) = A(k)\xi(k) + B(k)u(k), \tag{6}$$

where $A(k) = I + TA(t)$; $B(k) = TB(t)$; T is the sampling period; t is the sampling time; N_p is the prediction time domain; $K = t, t+1, \ldots\ldots, t+N_p$; I is the unit matrix.

In order to control the stability of the process, the change value of the front wheel angle is set as the output of the MPC controller, and a new state space expression is obtained:

$$\begin{cases} \tilde{\xi}(k+1|t) = \tilde{A}_{k,t}\tilde{\xi}(k|t) + \tilde{B}_{k,t}\Delta u(k|t), \\ \tilde{\lambda}(k|t) = \tilde{C}_{k,t}\tilde{\xi}(k|t), \end{cases} \tag{7}$$

where $\tilde{\xi}(k)$ is the state matrix composed of the state quantity at time k and the control quantity at time $k-1$,

$\widetilde{\xi}(k|t) = \begin{bmatrix} \xi(k|t) \\ u(k-1|t) \end{bmatrix}$; $\Delta u(k|t)$ is the control increment at time k of the system, $\Delta u(k|t) = u(k|t) - u(k-1|t)$; $\widetilde{A}_{k,t} = \begin{bmatrix} A_{k,t} & B_{k,t} \\ 0 & I \end{bmatrix}$, $\widetilde{B}_{k,t} = \begin{bmatrix} B_{k,t} \\ I \end{bmatrix}$; $\widetilde{\lambda}(k|t)$ is the output of the system at time k.

Assume that the prediction time domain of the MPC controller is Np, the control step size is Nc, and $Nc \le Np$. The predicted output of the system at time k is obtained as:

$$Y(k|t) = \psi_k \widetilde{\xi}(k|t) + \Theta_k \Delta U(k|t), \tag{8}$$

where $Y(k|t)$ is the output matrix in the prediction time domain, $Y(k) = \begin{bmatrix} \widetilde{\lambda}(k+1|t) \\ \widetilde{\lambda}(k+2|t) \\ \vdots \\ \widetilde{\lambda}(k+N_p|t) \end{bmatrix}$; $\Delta U(k)$ is the control increment in the control time domain Nc,

$$\Delta U(k) = \begin{bmatrix} \Delta u(k|t) \\ \Delta u(k+1|t) \\ \vdots \\ \Delta u(k+N_c-1|t) \end{bmatrix};$$

$$\psi_k = \begin{bmatrix} \widetilde{C}_{k,t}\widetilde{A}_{k,t} \\ \widetilde{C}_{k,t}\widetilde{A}^2_{k,t} \\ \vdots \\ \widetilde{C}_{k,t}\widetilde{A}^{N_p}_{k,t} \end{bmatrix};$$

$$\Theta_k = \begin{bmatrix} \widetilde{C}_{k,t}\widetilde{B}_{k,t} & 0 & \cdots & 0 \\ \widetilde{C}_{k,t}\widetilde{A}_{k,t}\widetilde{B}_{k,t} & \widetilde{C}_{k,t}\widetilde{B}_{k,t} & \cdots & 0 \\ \vdots & \vdots & \vdots & \vdots \\ \widetilde{C}_{k,t}\widetilde{A}^{N_c-1}_{k,t}\widetilde{B}_{k,t} & \widetilde{C}_{k,t}\widetilde{A}^{N_c-2}_{k,t}\widetilde{B}_{k,t} & \cdots & \widetilde{C}_{k,t}\widetilde{B}_{k,t} \\ \widetilde{C}_{k,t}\widetilde{A}^{N_c}_{k,t}\widetilde{B}_{k,t} & \widetilde{C}_{k,t}\widetilde{A}^{N_c-2}_{k,t}\widetilde{B}_{k,t} & \cdots & \widetilde{C}_{k,t}\widetilde{A}_{k,t}\widetilde{B}_{k,t} \\ \vdots & \vdots & \ddots & \vdots \\ \widetilde{C}_{k,t}\widetilde{A}^{N_p-1}_{k,t}\widetilde{B}_{k,t} & \widetilde{C}_{k,t}\widetilde{A}^{N_p-2}_{k,t}\widetilde{B}_{k,t} & \cdots & \widetilde{C}_{k,t}\widetilde{A}^{N_p-N_c-1}_{k,t}\widetilde{B}_{k,t} \end{bmatrix}. \tag{9}$$

The objective function is to ensure that the vehicle can track the desired trajectory with the smallest error, and the tracking process must be fast and stable. The objective function of the controller is designed as:

$$J = \sum_{i=1}^{N_p} \left\| \lambda(k+i|t) - \lambda_{\text{ref}}(k+i|t) \right\|^2_Q + \sum_{i=1}^{N_c-1} \left\| \Delta u(k+i|t) \right\|^2_R + \rho\varepsilon^2, \tag{10}$$

where $\lambda(k+i|t)$ is the actual output of the system; $\lambda_{\text{ref}}(k+i|t)$ is the reference output for the system; Q, R is the weight coefficient matrix; ρ is the relaxation factor weight coefficient; and ε is the relaxation factor.

In order to track the desired trajectory more accurately, the necessary dynamic constraints need to be added to the controller. Set the center of mass slip angle constraint to $-12^\circ \le \beta \le 12^\circ$, the attachment condition is constrained to $\sqrt{a_x^2 + a_y^2} \le \mu g$, μ is the ground friction coefficient, in order to prevent the constraint condition from being too small to cause no solution; a relaxation factor can be introduced to define the attachment condition constraint as a soft constraint: $a_{y,\min} - \varepsilon \le a_y \le a_{y,\max} + \varepsilon$; at the same time, the change range of the front wheel rotation angle is constrained to $-15^\circ \le \delta_f \le 15^\circ$; the angle change is $-0.8^\circ \le \Delta\delta_f \le 0.8^\circ$.

In order to solve the objective function using the quadratic programming method, it is necessary to convert the objective function to the standard form of the quadratic form:

$$J = \frac{1}{2}[\Delta U(k), \varepsilon]^T H [\Delta U(k), \varepsilon] + G[\Delta U(k), \varepsilon]^T, \tag{11}$$

where H,G is the coefficient matrix, $H = \begin{bmatrix} 2(\Theta_k^T Q \Theta_K + R) & 0 \\ 0 & 2\rho \end{bmatrix}$; $G = \begin{bmatrix} 2E^T(k) Q \Theta_k & 0 \end{bmatrix}$; $E(k)$ is the output deviation matrix in the prediction time domain.

By adding the dynamic constraints of the vehicle, the optimal control increment of the system under the constraints at each moment can be obtained through quadratic programming:

$$\begin{cases} \min\limits_{\Delta u(k),\varepsilon} & \frac{1}{2}[\Delta U(k), \varepsilon]^T H [\Delta U(k), \varepsilon] + G[\Delta U(k), \varepsilon]^T, \\ & \Delta U_{\min} \le \Delta U_t \le \Delta U_{\max}, \\ & U_{\min} \le U_t \le U_{\max}, \\ \text{s.t.} & \\ & y_{hc,\min} \le y_{hc} \le y_{hc,\max}, \\ & y_{sc,\min} - \varepsilon \le y_{sc} \le y_{sc,\max} + \varepsilon, \end{cases} \tag{12}$$

where y_{hc}, y_{sc} are hard and soft constraints, respectively.

In each sampling period, solve (11), we can get:

$$\Delta U^*(k) = \left[\Delta u^*(k), \Delta u^*(k+1|t), \ldots, \Delta u^*(k+N_c-1|t)\right]^T, \tag{13}$$

where $\Delta u^*(k), \Delta u^*(k+1|t), \ldots, \Delta u^*(k+N_c-1|t)$ is the system control input at time $k, k+1, \ldots, k+N_c-1$.

The first element of the incremental sequence is used as the control incremental input of the actual system to achieve rolling optimization and finally obtain the control amount $u(k)$:

$$u(k) = u(k-1) + \Delta u^*(k). \tag{14}$$

3.2. Adaptive Model Predictive Control. The prediction time domain is an important parameter in model predictive control, which represents the prediction of the system's future time, too large or too small will affect the tracking effect. When the prediction time domain Np is large, the system can predict the state for a long time in the future, which means that the weight coefficient of the error farther away from the vehicle is larger, and the weight of the current

error is smaller. Therefore, the vehicle will have a large error in the current position. When the prediction time domain Np is small, the system is more concerned about the error of the current moment, but due to the small prediction of the future moment and the related constraints of the steering wheel, the vehicle will not turn in time and cannot track the path. At the same time, the longitudinal speed of the vehicle also affects the tracking effect of the vehicle. The higher the speed, the farther the system needs to predict the future moment, and the larger the prediction time domain is required [23, 24]. Therefore, in order to improve the accuracy of trajectory tracking, the prediction time domain Np should change with the change of vehicle speed.

In order to determine the relationship between the prediction time domain and the vehicle speed, the optimal prediction time domain Np corresponding to different vehicle speeds was verified through the co-simulation of CarSim and MATLAB/Simulink. First, five sets of different prediction time domain values are taken for comparison at a speed of 25 km/h. The simulation results are shown in Figure 3.

According to the test results, it can be seen that when the vehicle speed is 25 km/h, the expected path can be followed when the prediction time domain takes different values. However, with the increase of the prediction time domain, the lateral error and yaw angle error of trajectory tracking increase significantly. When the prediction time domain $Np = 10$, the lateral error and the yaw angle error are the smallest at this time; when the prediction time domain $Np = 26$, the lateral error and the yaw angle error are the largest at this time. Therefore, when the vehicle speed is 25 km/h, the tracking effect is the best when the prediction time domain $Np = 10$. In the same way, the trajectory tracking tests of different prediction time domains Np at 45 km/h, 60 km/h, 85 km/h, and 100 km/h were carried out, respectively, and the simulation data of the test were summarized in Table 1.

According to the test results, it can be concluded that with the increase of vehicle speed, the influence of the prediction time domain on the trajectory tracking effect becomes more and more obvious. When the vehicle speed is 45 km/h, the lateral error is the smallest when the prediction time domain $Np = 10$, but the yaw angle tracking error is larger than the prediction time domain $Np = 14$, indicating that the tracking process is relatively jittery; when the vehicle speed is 60 km/h and the prediction time domain $Np = 18$, the vehicle lateral error and yaw angle error are the smallest at this time. When the vehicle speed is 85 km/h and the prediction time domain is 10 or 14, the vehicle has completely failed to track the desired path, and a larger Np is required to track the desired path; when the vehicle speed is 100 km/h, the prediction time domain needs to reach 26 to track the path with an appropriate error. Set the control time domain step size of model predictive control to 10, because the minimum prediction cannot be smaller than the control time domain, so the minimum prediction time domain is 10. Therefore, according to the analysis of each group of test data, the best prediction time domain Np under different vehicle speeds is summarized in Table 2.

By fitting the data in the table through a fifth-order polynomial, the adaptive model predictive control that automatically adjusts the prediction time domain Np with the change of vehicle speed can be obtained. The best prediction time domain corresponding to different speeds is shown in Figure 4:

3.3. Longitudinal Controller Design. The longitudinal controller is designed based on sliding mode variable structure control theory. Sliding mode variable structure control has a good effect on dealing with the uncertainty of nonlinear systems, and has the characteristic that the "structure" of system control is not unique, and the system can change according to real-time state changes. Moreover, the sliding mode variable structure control is not affected by the parameters of the object, the response speed is fast, and the robustness is strong, and can play a good control effect on the longitudinal speed varying at any time.

The core content of traditional sliding mode variable structure control is divided into two steps: one is to design the sliding mode region, so that the system has certain desired characteristics along the sliding mode trajectory; second, a discontinuous control is designed so that the trajectory of the system can reach the sliding mode region in finite time. In general, the state space equation of the system can be expressed as:

$$\dot{x} = f(x, u, t), \quad x \in R^n, u \in R^m, t \in R. \tag{15}$$

There is a hypersurface $s(x) = s(x_1, x_2 \ldots, x_n) = 0$ in the state space, which divides the state space into three cases: $s > 0$, $s < 0$ and $s = 0$, as shown in Figure 5.

In the figure, A represents the normal point, B represents the starting point, and C is the termination point. Only the termination point is meaningful in the sliding mode variable structure control. According to the definition of sliding mode variable structure control, all motion points in the sliding mode region need to reach the termination point condition, and we can get:

$$\begin{aligned} \lim_{s \longrightarrow 0^+} \dot{s} \leq 0, \\ \lim_{s \longrightarrow 0^-} \dot{s} \geq 0. \end{aligned} \tag{16}$$

It can also be further expressed as:

$$\lim_{s \longrightarrow 0} \dot{s}s \leq 0. \tag{17}$$

This forms the necessary condition for the Lyapunov function of the form $v(x_1, x_2 \ldots, x_n) = s[s(x_1, x_2 \ldots, x_n)]^2$. Since formula (17) of the sliding mode neighborhood is positive definite, and the first derivative is negative semidefinite, therefore, the necessary conditions of the Lyapunov function are satisfied, and the system itself tends to be stable under the condition of $s = 0$. However, the sliding mode variable structure control is essentially a discontinuous switching property, which will lead to the phenomenon of jitter in the system. In the actual phenomenon, this kind of jitter is difficult to eliminate, and can only be weakened by relevant methods.

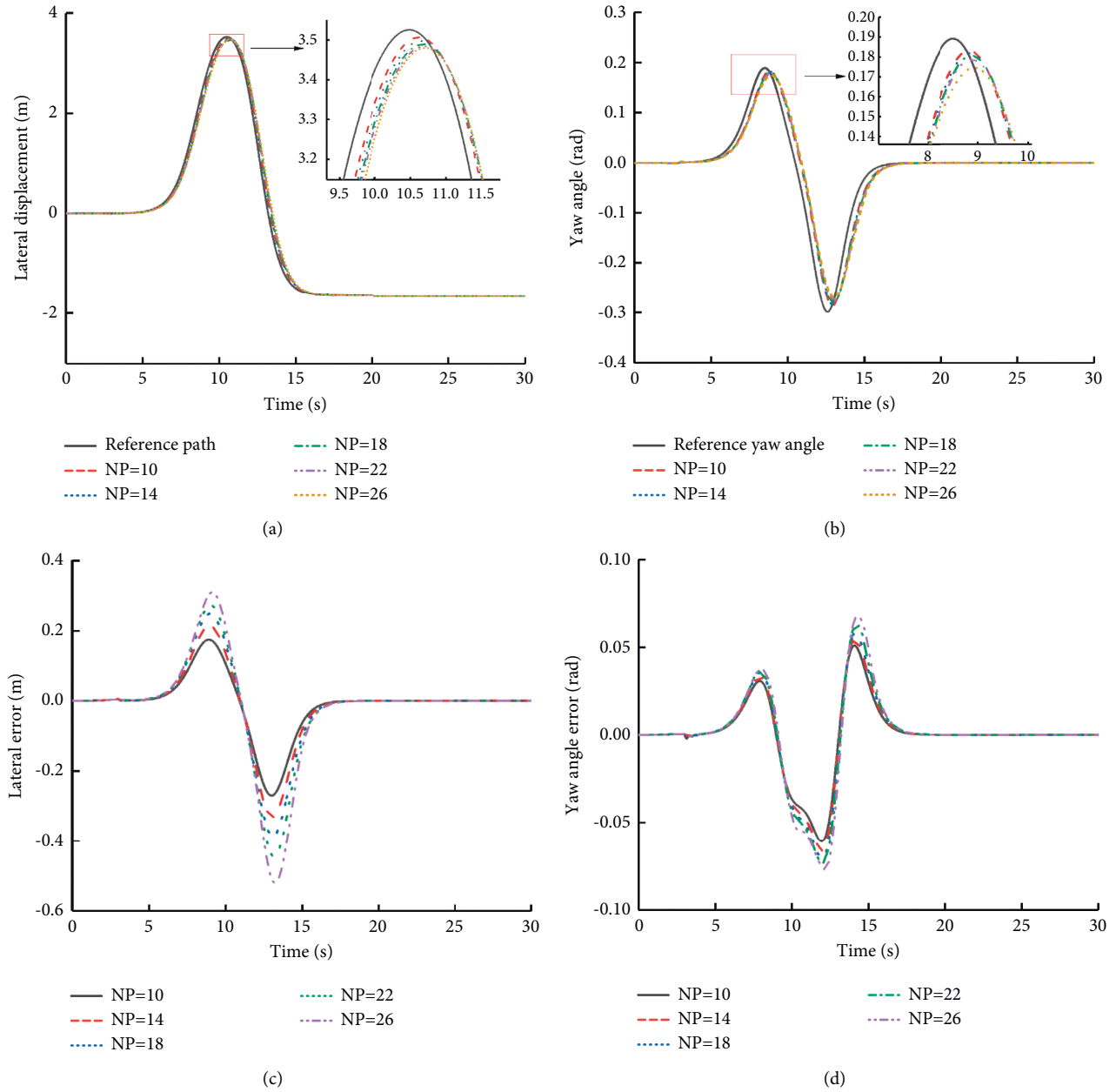

Figure 3: Simulation results at different speeds. (a) Lateral position tracking comparison. (b) Yaw angle tracking comparison. (c) Lateral tracking error. (d) Yaw angle tracking error.

Table 1: Simulation data for different vehicle speeds.

Np	v = 45 km/h		v = 60 km/h		v = 85 km/h		v = 100 km/h	
	Δy_{max} (m)	$\Delta\varphi_{max}$ (rad)	Δy_{max} (m)	$\Delta\varphi_{max}$ (rad)	Δy_{max} (m)	$\Delta\varphi_{max}$ (rad)	Δy_{max} (m)	$\Delta\varphi_{max}$ (rad)
10	0.413	0.067	0.599	0.081	—	—	—	—
14	0.419	0.061	0.566	0.076	—	—	—	—
18	0.482	0.072	0.559	0.070	0.603	0.077	—	—
22	0.509	0.073	0.575	0.079	0.601	0.073	0.653	0.086
26	0.541	0.079	0.603	0.082	0.663	0.079	0.602	0.073

In the tracking process of the longitudinal speed, the vehicle is required to be able to smoothly accelerate and decelerate, and the influence of the lateral motion on the longitudinal speed needs to be considered. In order to better track the desired vehicle speed, the upper and lower controllers jointly control the longitudinal speed of the car; the

Table 2: Prediction time domain corresponding to different vehicle speeds.

Speed (km/h)	20	25	45	60	85	100
Prediction time domain (Np)	10	10	14	18	22	26

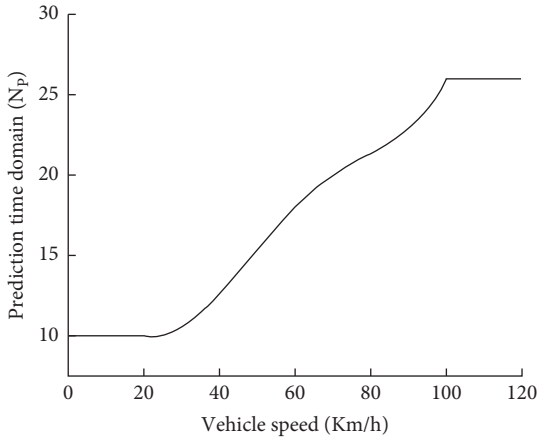

Figure 4: The best prediction time domain corresponding to different vehicle speeds.

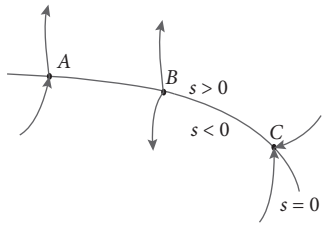

Figure 5: Sliding modal motion point state.

upper controller calculates the resultant torque of the racing car, the lower controller sets the switching logic to realize driving and braking according to the magnitude of the resultant torque and the additional yaw moment. After the calculation of the upper controller and the control of the wire control device of the lower controller work together to achieve the purpose of tracking the desired vehicle speed, its principle structure is shown in Figure 6.

According to the established three-degree-of-freedom dynamic model of the vehicle, the longitudinal force of the vehicle is analyzed:

$$m\ddot{x} = 2\left(F_{lf}\cos\delta_f - F_{cf}\sin\delta_f\right) + 2F_{lr} + mv_y\omega. \tag{18}$$

Meanwhile, according to the car driving equation:

$$F_t = F_f + F_w + F_i + F_j, \tag{19}$$

where F_t is the driving force; F_f is the rolling resistance; F_w is the air resistance; F_i is the ramp resistance; and F_j is the acceleration resistance.

Since the race car runs on a good road without ramps, the slope resistance is ignored; meanwhile, the air resistance and acceleration resistance have little influence on the race car, and the air resistance and acceleration resistance are ignored. After derivation, we get:

$$\ddot{x} = \frac{Ti}{mR} - \frac{2}{m}C_{cf}\left(\delta_f - \frac{\dot{y} + a\dot{\varphi}}{\dot{x}}\right) + \dot{y}\dot{\varphi} - f_R g, \tag{20}$$

where T is the resultant torque, indicating the driving torque or braking torque; i is the main reducer gear ratio; R is the effective radius of the wheel; and f_R is the rolling resistance coefficient.

The longitudinal speed tracking error of the vehicle is designed as a sliding mode switching function:

$$s = \dot{x}_d - \dot{x}, \tag{21}$$

where $\dot{x}_d$ is the expected longitudinal velocity; $\dot{x}$ is the actual longitudinal velocity. Further derivation:

$$\dot{s} = \ddot{x}_d - \ddot{x}. \tag{22}$$

Use the exponential approach rate:

$$\dot{s} = -\varepsilon\,\mathrm{sgn}(s) - ks, \quad \varepsilon > 0, k > 0, \tag{23}$$

where ε is the reaching law constant, k is the sliding mode control parameter.

In order to reduce the jitter in sliding mode control, the switching characteristics are approximately linearized, and the saturation function $\mathrm{sat}(s/\phi)$ is used to replace the sign function.

$$\mathrm{sat}\left(\frac{s}{\phi}\right) = \begin{cases} \mathrm{sgn}(s), & |s| \geq \phi, \\ \dfrac{s}{\phi}, & |s| < \phi, \end{cases} \quad \phi \in R, \phi > 0. \tag{24}$$

Combined (23) can obtain the resultant torque control rate:

$$T = \frac{2R}{i}C_{cf}\left(\delta_f - \frac{\dot{y} + a\dot{\varphi}}{\dot{x}}\right)\sin\delta_f + \frac{mR}{i}\left(\ddot{x}_d + f_R g + \varepsilon\,\mathrm{sat}(s) + ks\right). \tag{25}$$

4. Differential Drive Control

In order to reduce the trajectory tracking error of the racing car at high speed and improve the driving stability of the racing car, this paper decides to use differential drive control to control the driving torque of the racing car. Calculate the vehicle's expected yaw rate and center of mass slip angle according to the vehicle's current speed and front wheel angle, design a fuzzy controller based on fuzzy control theory, take the vehicle's yaw rate deviation and center of mass slip angle deviation as the input of the fuzzy controller, the additional yaw moment that can make the vehicle run stably is obtained by the fuzzy controller. Then, the driving torque and the additional yaw moment are redistributed, the driving torque due to

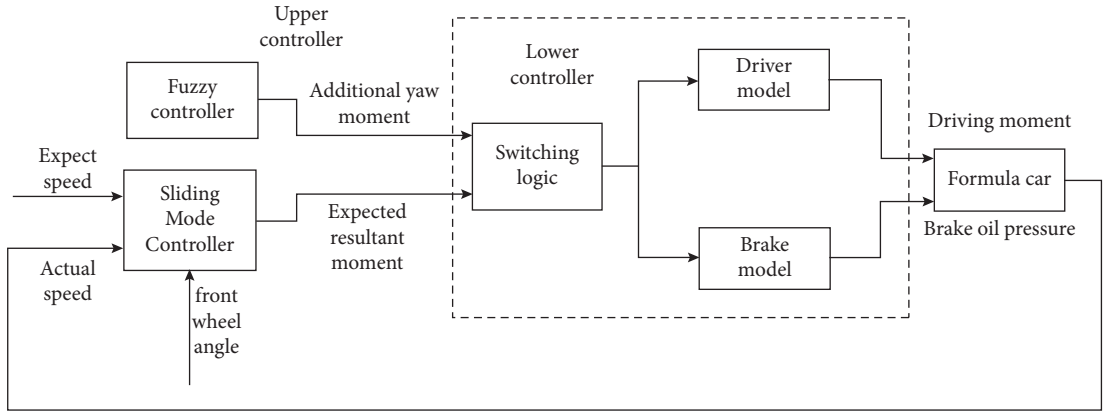

Figure 6: Longitudinal motion control principle.

each driving wheel is calculated, and this differential drive control is selected to control the additional yaw moment of the race car.

4.1. Reference Model. Calculate the vehicle's desired yaw rate and center of mass slip angle according to a linear two-degree-of-freedom vehicle model:

$$\omega_d = \frac{\dot{x}/L}{1 + K\dot{x}^2} \cdot \delta_f, \tag{26}$$

$$\beta_d = \frac{b + am\dot{x}^2/C_r L}{\left(1 + K\dot{x}^2\right)/L} \cdot \delta_f, \tag{27}$$

where ω_d is the steady-state value of the yaw angle; β_d is the steady-state value of the center of mass slip angle; L is the wheelbase; a, b is the distance from the front and rear axles of the car to the center of mass, respectively; C_r, C_f is the front and rear axle cornering stiffness, respectively; stability factor $K = m/L^2\,(a/C_r - b/C_f)$.

The linear two-degree-of-freedom model of vehicle limits the tire's side deflection characteristics within the linear range. When the tire works in the nonlinear region, the yaw rate and center of mass slip angle calculated by (26) and (27) cannot meet the stability requirements of the vehicle; therefore, it is necessary to design the critical expected value, and the critical value of the design expected yaw rate and the center of mass slip angle is:

$$\begin{aligned} \omega_b &= 0.85\frac{\mu g}{\dot{x}}, \\ \beta_b &= \arctan\left(0.02\mu g\right), \end{aligned} \tag{28}$$

where μ is the road adhesion coefficient; g is the acceleration of gravity.

4.2. Fuzzy Controller Design. The difference between steady yaw rate, steady center of mass slip angle, and the actual yaw rate and center of mass slip angle was taken as the input of the fuzzy controller, the additional yaw moment ΔM is used as the output of the controller. Set the fuzzy domain of yaw rate deviation and center of mass slip angle deviation as [−3, 3], the fuzzy subset of input linguistic variables is the $\{NB, NS, ZO, PS, PB\}$. The fuzzy domain of the additional yaw moment is set to [−50, 50], the fuzzy subset of output linguistic variables is the $\{NB, NM, NS, ZO, PS, PM, PB\}$. The membership functions of the input and output are shown in Figures 7 and 8.

According to the vehicle dynamics theory and simulation experience, when the vehicle is understeering, the yaw moment in the same direction should be applied to the vehicle, and when the vehicle is oversteering, the opposite yaw moment should be applied. The fuzzy control rules are formulated as shown in Table 3:

The fuzzy inference is fuzzified by the Mamdani method, and the output surface graph of the additional yaw moment is obtained, as shown in Figure 9.

4.3. Moment Redistribution. The additional yaw moment calculated by the fuzzy controller needs to be distributed to different driving wheels according to the rules. When the vehicle appears to be under-steering to the left or over-steering to the right, it is necessary to increase the torque of the right drive wheel and reduce the torque of the left drive wheel, so that the drive wheels on each side generate half of the additional yaw moment:

$$\begin{cases} T_L = T - \dfrac{1}{2}|\Delta M| \cdot \dfrac{r}{(B/2)}, \\ T_R = T + \dfrac{1}{2}|\Delta M| \cdot \dfrac{r}{(B/2)}, \end{cases} \tag{29}$$

where T_L, T_R is the left and right drive wheel torque after distribution, respectively; T is the resultant torque of the drive motor before distribution; B is the Wheelbase of the rear axle.

When the vehicle is under-steering to the right or over-steering to the left, the desired yaw rate at this time is less than the actual yaw rate, and it is necessary to increase the driving torque of the left driving wheel and reduce the driving torque of the right driving wheel, and obtain:

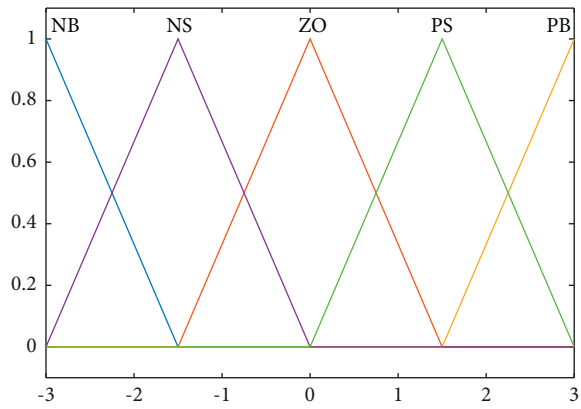

Figure 7: The membership function of $\Delta\omega$, $\Delta\beta$.

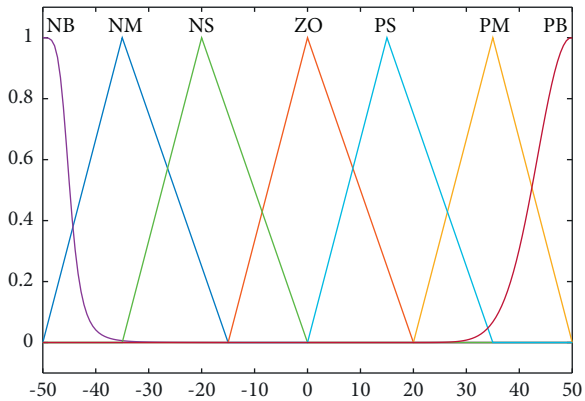

Figure 8: The membership function of ΔM.

Table 3: Fuzzy control rule table.

		$\Delta\omega$				
		NB	NS	ZO	PS	PB
$\Delta\beta$	NB	PB	PB	NS	NB	NB
	NS	PB	PM	NS	NM	NB
	ZO	PM	PS	ZO	NS	NM
	PS	PM	PM	PS	NM	NB
	PM	PB	PS	PS	NS	NB

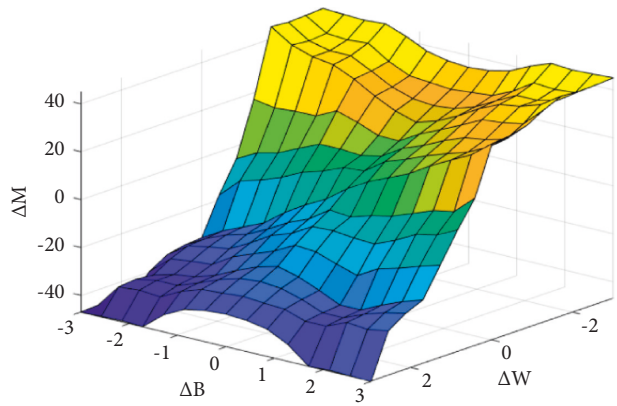

Figure 9: Additional yaw moment output surface plot.

Table 4: Main parameters of the race car.

Symbol	Parameters (units)	Value
m	Vehicle mass (kg)	260
a	Distance from the center of mass to the front axis (mm)	706.5
b	Distance from the center of mass to the rear axis (mm)	863.5
l	Wheelbase of vehicle (mm)	1570
h_g	Height of the center of mass (mm)	270
R	Effective radius of wheel (mm)	228.6
T_f	Wheelbase of the front axle (mm)	1200
T_r	Wheelbase of the rear axle (mm)	1180

$$\begin{cases} T_L = T + \dfrac{1}{2}|\Delta M| \cdot \dfrac{r}{(B/2)}, \\ T_R = T - \dfrac{1}{2}|\Delta M| \cdot \dfrac{r}{(B/2)}. \end{cases} \tag{30}$$

5. Simulation Verification Results

CarSim and MATLAB/Simulink are used to conduct co-simulation to verify the effectiveness of the lateral and longitudinal coordinated control strategy proposed in this paper. The main parameters of the driverless formula car model are shown in Table 4.

The high-speed tracking project has a complex track with many curves and complex and changeable curvatures. In order to verify the effectiveness of the designed lateral and longitudinal coordinated control strategy, it is necessary to establish a relatively complex expected driving trajectory. At the same time, the race car needs to accelerate and decelerate according to the road conditions in the process of driving. In the straight line driving condition, it is necessary to give full play to the acceleration performance of the race car to achieve the maximum longitudinal speed at the fastest speed, and according to the actual braking performance of the race car, before reaching the next corner, decelerate to reach the expected speed of the corner. According to the established reference trajectory and simulation test, the expected vehicle speed is designed. The maximum allowable vehicle speed when turning is defined as:

$$v_{\max} = \sqrt{\frac{g\mu}{\rho}}, \tag{31}$$

where ρ is the road curvature; the road curvature can be represented by the desired lateral position:

$$\rho = \frac{Y''_{\text{ref}}(X)}{\sqrt[3/2]{\left(1 + \left(Y'_{\text{ref}}(X)\right)^2\right)}}. \tag{32}$$

In order to verify the effectiveness and robustness of the designed lateral and longitudinal coordinated control strategy, simulation was carried out on the road surfaces with high and low road adhesion coefficients, respectively. The effectiveness of the lateral and longitudinal coordinated

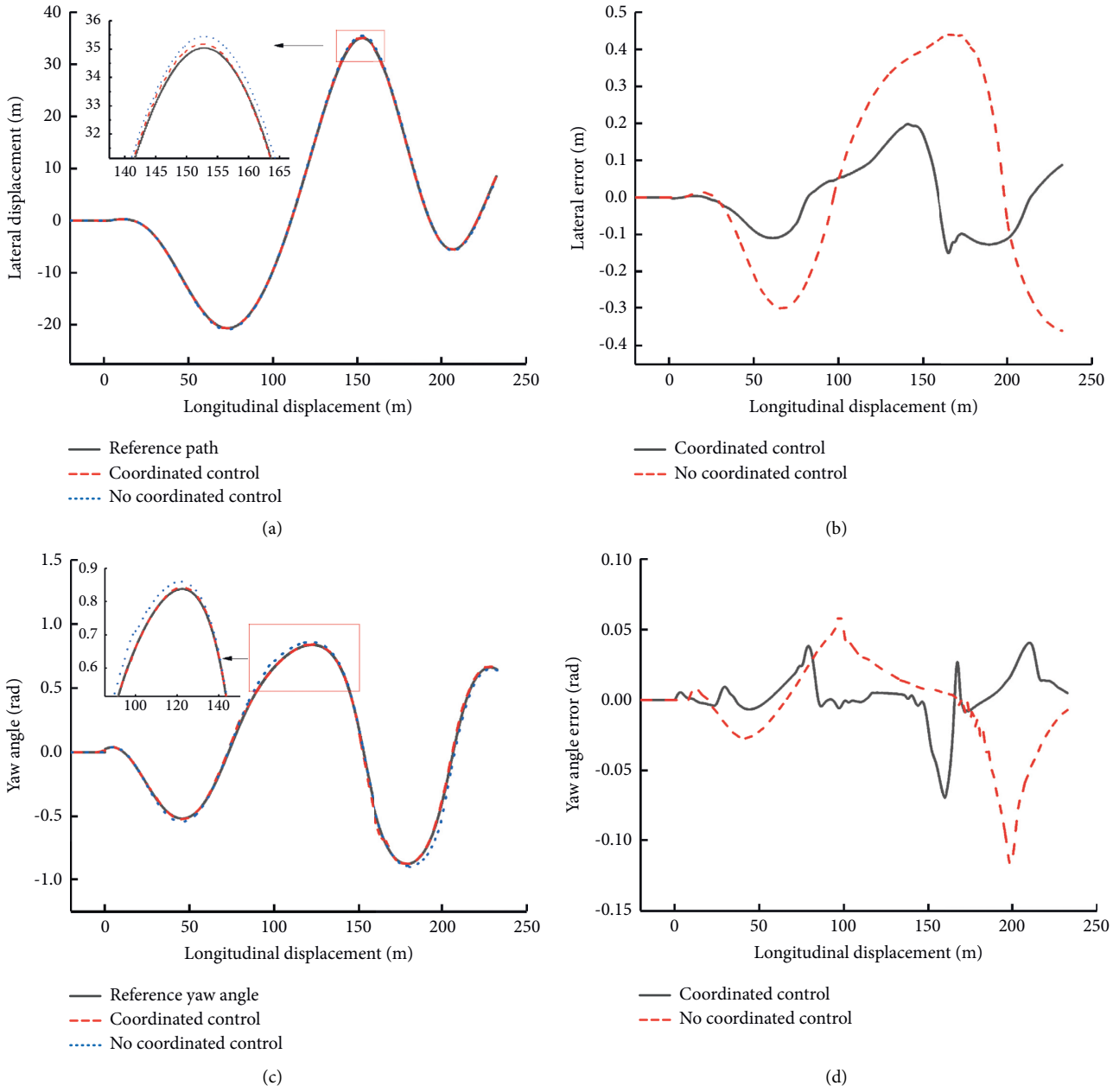

Figure 10: Continued.

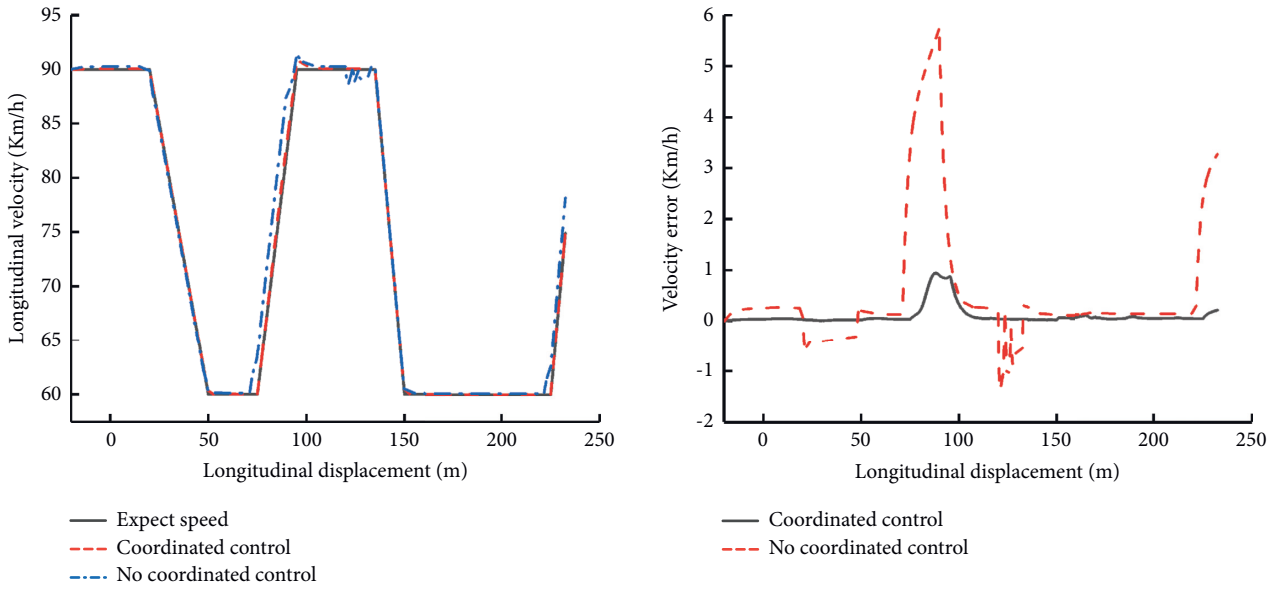

Figure 10: Simulation results of high adhesion coefficient. (a) Lateral position tracking comparison. (b) Lateral position tracking error. (c) Yaw angle tracking comparison. (d) Yaw angle tracking error. (e) Longitudinal speed tracking comparison. (f) Longitudinal speed tracking error.

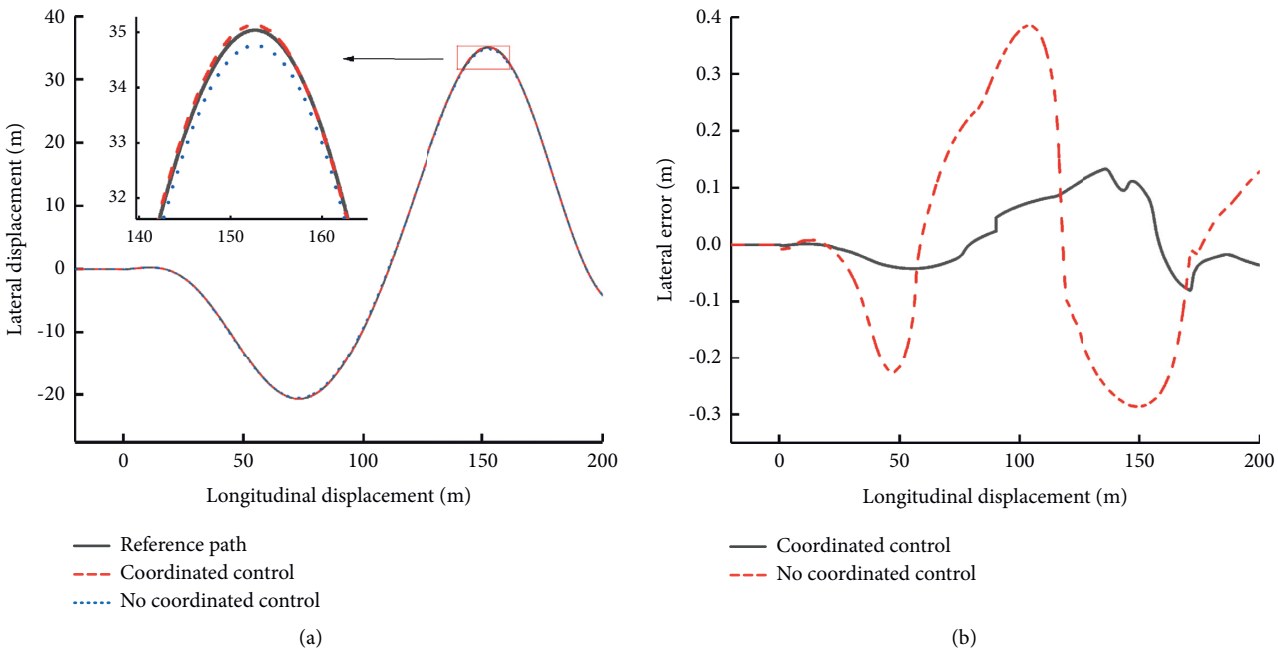

Figure 11: Continued.

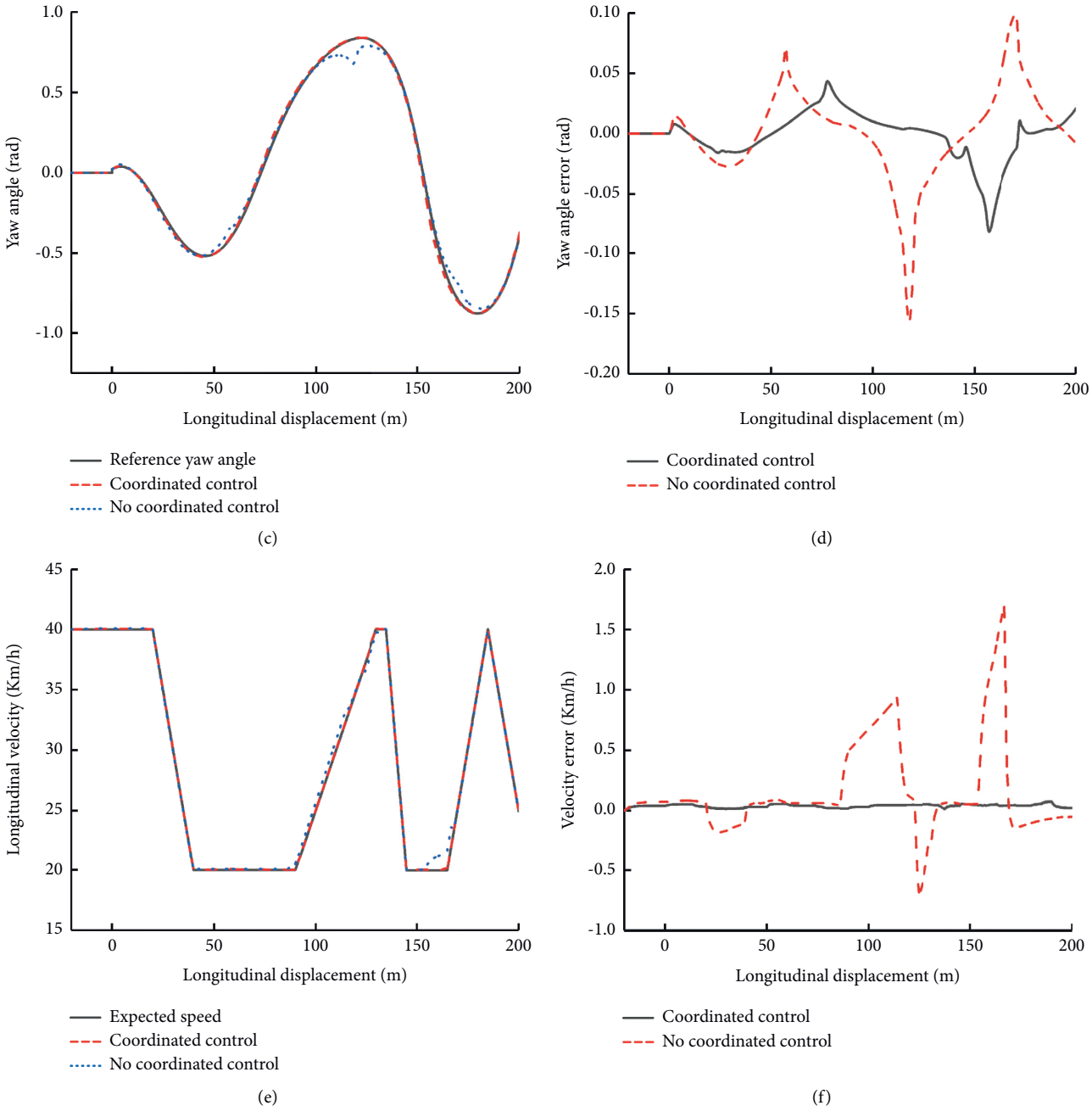

Figure 11: Simulation results of low adhesion coefficient. (a) Lateral position tracking comparison. (b) Lateral position tracking error. (c) Yaw angle tracking comparison. (d) Yaw angle tracking error. (e) Longitudinal speed tracking comparison. (f) Longitudinal speed tracking error.

control strategy is verified by comparing it with a racing car without lateral and longitudinal coordinated control that does not consider the interaction between the lateral and longitudinal directions.

5.1. High Adhesion Coefficient Pavement Test. In this simulation environment, the road adhesion coefficient is set to 0.85, the initial speed of the car is 90 km/h, and the maximum speed is 90 km/h. The simulation condition selects the high-speed tracking condition, and the simulation results are shown in Figure 10.

From Figures 10(a)–10(f), it can be seen that when the race car is running at high speed on the high-adhesion road, the tracking effect of the lateral position and longitudinal speed of the race car with the coordinated control strategy is better than that without the coordinated control. It can be seen from Figures 10(a) and 10(b) that the maximum lateral error of tracking without coordinated control is about 0.45 m, while the coordinated control can make the lateral error within about 0.2 m, effectively reducing the lateral tracking error; from Figures 10(c) and 10(d), it can be seen that the tracking effect of the yaw angle

with the coordinated control is better than that without the coordinated control, and the yaw angle error without the coordinated control can reach 0.12 rad in the curve around 200 m; it will cause a lot of jitters, but through the lateral and longitudinal coordinated control, even in the curve, the maximum yaw angle error of the vehicle is 0.07 rad, and the tracking effect is good; it can be seen from Figures 10(e) and 10(f) that, in the longitudinal expected speed tracking process, the race car without coordinated control will produce obvious errors when the speed changes. The race car without coordinated control will produce a speed error of about 5.7 km/h in the process of cornering acceleration, while the race car with coordinated control will only produce a speed error of 1 km/h. The speed error of other sections fluctuates around 0 km/h, and the longitudinal speed tracking accuracy is very high. Therefore, on the road surface with high adhesion coefficient, the proposed lateral and longitudinal coordinated control strategy has a good tracking effect, which not only reduces the lateral tracking error but also greatly reduces the longitudinal tracking error.

5.2. Low Adhesion Coefficient Pavement Test. In this simulation environment, the road adhesion coefficient is set to 0.3, the initial speed is 40 km/h, and the maximum speed is 40 km/h. The simulation condition selects the high-speed tracking condition, and the simulation results are shown in Figure 11.

It can be seen from Figures 11(a)–11(f) that the tracking effect of the race car with the coordinated control strategy is obviously better than that without the coordinated control. As can be seen from Figures 11(a) and 11(b), due to the low road adhesion coefficient, the ultimate adhesion of the race car without coordinated control is also small. In the cornering process, the maximum lateral tracking error reaches 0.39 m, while the maximum lateral error of the race car with coordinated control is about 0.13 m. The average lateral error is within about 0.05 m; it can be seen from Figures 11(c) and 11(d) that the yaw angle tracking error of the race car without coordinated control fluctuates greatly, and the maximum yaw angle error reaches 0.16 rad, while the maximum yaw angle error with coordinated control is about 0.08 rad; as can be seen from Figures 11(e) and 11(f), the speed change of the race car without coordinated control will have obvious jitter. Due to the low speed of the race car, the speed error of the race car without coordinated control is also lower, and the maximum longitudinal speed error is 1.7 km/h, and the average longitudinal speed error is about 0.3 km/h, but the longitudinal speed error of the race car with the coordinated control strategy is almost 0 in the whole process, and the average longitudinal speed error is about 0.04 km/h. Therefore, on the road with low adhesion coefficient, the proposed lateral and longitudinal coordinated control strategy still has a good tracking effect.

6. Conclusions

Aiming at the problem of low track tracking control accuracy of distributed driven driverless racing car under high-speed tracking conditions, this paper proposes a lateral and longitudinal coordinated control strategy, and the following conclusions can be drawn:

(1) Aiming at the lateral motion control of distributed driven driverless racing car under variable speed driving conditions, a lateral motion control algorithm is designed by applying adaptive model predictive control theory, and the controller prediction time domain is changed in real time according to the change of vehicle speed, the co-simulation test verified that the algorithm could effectively improve the trajectory tracking control accuracy.

(2) Aiming at the trajectory tracking control of distributed driven driverless racing car under high-speed tracking condition, a lateral and longitudinal coordinated control strategy was proposed, the lateral motion control took into account the influence of longitudinal speed and longitudinal displacement, the longitudinal motion control took into account the influence of front wheel angle, the driving torque was reasonably distributed through differential drive control, and the co-simulation results show that the control strategy can effectively improve the trajectory tracking control accuracy and driving stability.

Meanwhile, there are some limitations to this study. In the current study, when the vehicle is running at a high speed, the accuracy of tracking the desired path of the racing car is low, and the driving stability of the racing car is poor, and there will be obvious jitter. In the future, we will conduct experiments on real vehicles to verify the effectiveness of the coordinated control strategy. In addition, we will improve the vehicle stability control method. The differential drive control based on fuzzy control theory adopted in this paper will produce certain errors at high speed, so it can be considered to combine with other stability control methods to improve the trajectory tracking control accuracy and improve the vehicle driving stability.

Data Availability

The data used to support the findings of this study are available from the corresponding author upon request.

Conflicts of Interest

The authors declare that they have no conflicts of interest.

Acknowledgments

This work was supported by the National Science Foundation of China (51675257, 51305190), General program of Natural Science Foundation of Liaoning Province in 2022(396), and "Liaoning BaiQianWan Talents Program."

References

[1] Y. Huang, H. Ding, Y. Zhang et al., "A motion planning and tracking framework for autonomous vehicles based on artificial potential field elaborated resistance network approach,"

IEEE Transactions on Industrial Electronics, vol. 67, no. 2, pp. 1376–1386, 2020.

[2] M. Elbanhawi, M. Simic, and R. Jazar, "Receding horizon lateral vehicle control for pure pursuit path tracking," *Journal of Vibration and Control*, vol. 24, no. 3, pp. 619–642, 2018.

[3] X. Lu, Y. Xing, Z. Guirong, L. Bo, and Z. Renxie, "Review on motion control of autonomous vehicles," *Journal of Mechanical Engineering*, vol. 56, no. 10, pp. 127–143, 2020.

[4] D. Zhao, X. Li, Y. Zhao et al., "Oleanolic acid exerts bone protective effects in ovariectomized mice by inhibiting osteoclastogenesis," *Journal of Pharmacological Sciences*, vol. 137, no. 1, pp. 76–85, 2018.

[5] K. Liu, J. Gong, S. Chen, Y. Zhang, and H. Chen, "Model predictive stabilization control of high-speed autonomous ground vehicles considering the effect of road topography," *Applied Sciences*, vol. 8, no. 5, pp. 822–837, 2018.

[6] N. Guo, X. Zhang, Y. Zou, G. Du, C. Wang, and L. Guo, "Predictive energy management of plug-in hybrid electric vehicles by real-time optimization and data-driven calibration," *IEEE Transactions on Vehicular Technology*, vol. 71, no. 6, pp. 5677–5691, 2022.

[7] C. G. Bobier and J. C. Gerdes, "Staying within the nullcline boundary for vehicle envelope control using a sliding surface," *Vehicle System Dynamics*, vol. 51, no. 2, pp. 199–217, 2013.

[8] I. Carlucho, M. De Paula, and G. G. Acosta, "An adaptive deep reinforcement learning approach for MIMO PID control of mobile robots," *ISA Transactions*, vol. 102, pp. 280–294, 2020.

[9] C. Zhang, J. Hu, J. Qiu, W. Yang, H. Sun, and Q. Chen, "A novel fuzzy observer-based steering control approach for path tracking in autonomous vehicles," *IEEE Transactions on Fuzzy Systems*, vol. 27, no. 2, pp. 1–290, 2018.

[10] N. R. Kapania and J. C. Gerdes, "Design of a feedback feedforward steering controller for accurate path tracking and stability at the limits of handling," *Vehicle System Dynamics*, vol. 53, no. 12, pp. 1687–1704, 2015.

[11] C. Pinto, I. Nieva, S. Mata, I. Cabanes, and A. Zubizarreta, "Linear time varying model based model predictive control for lateral path tracking," *International Journal of Vehicle Design*, vol. 75, no. 1/2/3/4, pp. 1–22, 2018.

[12] T. Novi, A. Liniger, R. Capitani, and C. Annicchiarico, "Real-time control for at-limit handling driving on a predefined path," *Vehicle System Dynamics*, vol. 58, no. 7, pp. 1007–1036, 2020.

[13] K. Zhang, Q. Sun, and Y. Shi, "Trajectory tracking control of autonomous ground vehicles using adaptive learning MPC," *IEEE Transactions on Neural Networks and Learning Systems*, vol. 32, no. 12, pp. 5554–5564, 2021.

[14] H. Kim, D. Kim, I. Shu, and K. Yi, "Time-varying parameter adaptive vehicle speed control," *IEEE Transactions on Vehicular Technology*, vol. 65, no. 2, pp. 581–588, 2016.

[15] E. Velenis and P. Tsiotras, "Minimum-time travel for a vehicle with acceleration limits: theoretical analysis and receding-horizon implementation," *Journal of Optimization Theory and Applications*, vol. 138, no. 2, pp. 275–296, 2008.

[16] M. Buechel and A. Knoll, "A parameter estimator for a model based adaptive control scheme for longitudinal control of automated vehicles," *IFAC-PapersOnLine*, vol. 49, no. 15, pp. 181–186, 2016.

[17] Y. Xu, W. Tang, B. Chen, L. Qiu, and R. Yang, "A model predictive control with preview-follower theory algorithm for trajectory tracking control in autonomous vehicles," *Symmetry*, vol. 13, no. 3, 2021.

[18] H. Xie and S. Liu, "Lateral and longitudinal motion control of unmanned vehicles using model predictive control," *Journal of Automotive Safety and Energy*, vol. 10, no. 3, pp. 326–343, 2019.

[19] X. Zhang and L. Li, "Lateral and longitudinal coordinated control for intelligent-electric-vehicle trajectory-tracking based on LQR-dual PID," *Journal of Automotive Safety and Energy*, vol. 12, no. 3, pp. 346–354, 2021.

[20] P. Qin, F. Wu, and S. Zhang, "Intelligent and connected platoon lateral and longitudinal coordinated control considering road conditions," *Science Technology and Engineering*, vol. 21, no. 3, pp. 1059–1065, 2021.

[21] L. Chen, K. Zhou, C. Teng, X. Sun, and H. Wang, "Longitudinal and lateral comprehensive trajectory tracking control of intelligent vehicles based on NMPC," *Automotive Engineering*, vol. 43, no. 2, pp. 153–161, 2021.

[22] D. S. Pae, G. H. Kim, T. K. Kang, and M. T. Lim, "Path planning based on obstacle-dependent Gaussian model predictive control for autonomous driving," *Applied Sciences*, vol. 11, no. 8, 2021.

[23] G. Bai, Y. Meng, and Q. Gu, "Path tracking control of vehicles based on variable prediction horizon and velocity," *China Mechanical Engineering*, vol. 31, no. 11, pp. 1277–1284, 2020.

[24] B. Sakhdari and N. L. Azad, "Adaptive tube-based nonlinear MPC for economic autonomous cruise control of plug-in hybrid electric vehicles," *IEEE Transactions on Vehicular Technology*, vol. 67, no. 12, Article ID 11390, 2018.